COMPUTING ISOTROPIC LOCAL CONTRAST FROM ORIENTED PYRAMID DECOMPOSITIONS

Stefan Winkler, Pierre Vandergheynst

Signal Processing Laboratory
Swiss Federal Institute of Technology
1015 Lausanne, Switzerland
http://ltswww.epfl.ch/
Stefan.Winkler@epfl.ch

ABSTRACT

Working with contrast instead of luminance can facilitate numerous image processing and analysis tasks. Unfortunately, a common definition of contrast suitable for all situations does not exist. In this paper we review existing contrast definitions for natural images and propose a new isotropic contrast measure, which is computed from oriented filters. We investigate some of its properties and apply it to natural images.

1. GLOBAL CONTRAST

The response of the human visual system depends much less on the absolute luminance than on the relation of its local variations to the surrounding luminance. This property is known as *Weber's law*. Contrast is a measure of this relative variation of luminance.* Unfortunately, a common definition of contrast suitable for all situations does not exist, not even for simple stimuli. Mathematically, *Weber contrast* can be expressed as

$$C^W = \frac{\Delta L}{L}.$$

In vision experiments, this definition is used mainly for patterns consisting of a single increment or decrement ΔL to an otherwise uniform background luminance. In the case of sinusoids or other periodic patterns of symmetrical deviations ranging from $L_{\min}$ to $L_{\max}$, which are very popular in psychophysics, *Michelson contrast* [5] is generally used:

$$C^M = \frac{L_{\max} - L_{\min}}{L_{\max} + L_{\min}}.$$

These two definitions are by no means equivalent and do not even share a common range of values: Michelson contrast can range from 0 to 1, whereas Weber contrast can range from -1 to ∞.

2. LOCAL CONTRAST

While the above-mentioned definitions are good predictors of perceived contrast for simple stimuli such as sinusoids, they fail when stimuli become more complex and cover a wider frequency range, for example Gabor patches [8]. It is also evident that none of these simple global definitions is appropriate for measuring contrast in natural images, because a few very bright or very dark points would determine the contrast of the whole image. Essentially, human contrast sensitivity varies with the *local* average luminance. In order to address these issues, Peli [7] proposed a local band-limited contrast measure:

$$C_j^P(x,y) = \frac{\mathrm{bp}_j(x,y)}{\mathrm{lp}_{j+1}(x,y)}, \tag{1}$$

where $\mathrm{bp}_j(x,y)$ is the band-pass filtered image of band j, and $\mathrm{lp}_{j+1}(x,y)$ contains the energy below this band.

An important point is that this contrast measure is well defined if certain conditions are imposed on the filter kernels. Let us call k_{bp} and k_{lp} the kernels used to compute bp and lp respectively. If we assume that the signal and k_{lp} are positive real-valued integrable functions and k_{lp} is integrable, $C_j^P(x,y)$ is a well defined quantity provided that the (essential) support of k_{bp} is included in the (essential) support of k_{lp}. In this case $\mathrm{lp}_j(x,y) = 0$ implies $C_j^P(x,y) = 0$.

The band-pass filters of a pyramid transform that permits perfect reconstruction (see appendix) can also be computed as the difference of two neighboring low-pass filters. Hence Eq. (1) can be rewritten as

$$C_j^P(x,y) = \frac{\mathrm{lp}_j(x,y) - \mathrm{lp}_{j+1}(x,y)}{\mathrm{lp}_{j+1}(x,y)} = \frac{\mathrm{lp}_j(x,y)}{\mathrm{lp}_{j+1}(x,y)} - 1.$$

Lubin [3] used the following modification of Peli's contrast definition in an image quality metric based on a multichannel model of the human visual system:

$$C_j^L(x,y) = \frac{\mathrm{lp}_j(x,y) - \mathrm{lp}_{j+1}(x,y)}{\mathrm{lp}_{j+2}(x,y)}.$$

Here, the averaging low-pass has moved down one level. This particular local band-limited contrast definition has been found to be in good agreement with psychophysical contrast-matching experiments with Gabor patches [8].

* While Weber's law is only an approximation of the actual sensory perception, contrast measures based on this concept are widely used in vision science.

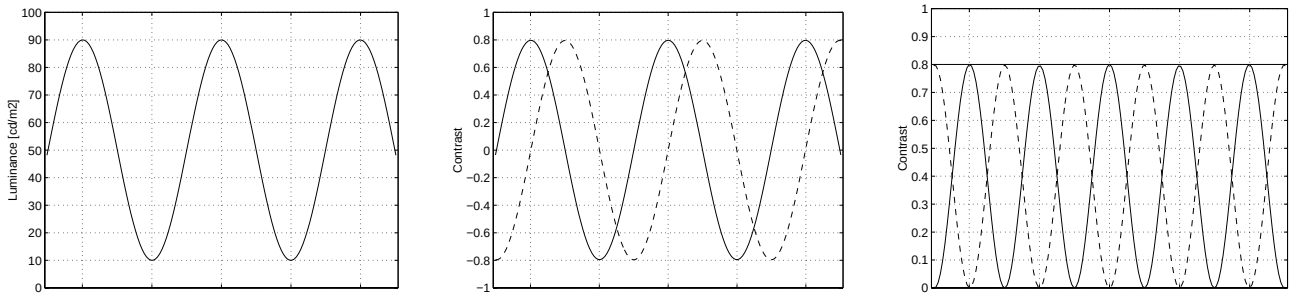

Figure 1: Sinusoid grating with $C^M = 0.8$ (left), normalized responses of in-phase (solid) and quadrature (dashed) filters (center), and respective normalized energy responses (right), whose sum is constant.

We note that the differences between C^P and C^L are most pronounced for the higher-frequency bands. The lower one goes, the more spatially uniform the low-pass band in the denominator will become in both measures, finally approaching the overall luminance mean of the image. Peli's definition exhibits relatively high overshoots in certain image regions, however, which is mainly due to the spectral proximity of the band-pass and low-pass filters.

3. IN-PHASE AND QUADRATURE MECHANISMS

C^P and C^L as defined above measure contrast only as incremental or decremental changes from the local background, which is analogous to the symmetric (in-phase) responses of vision mechanisms. However, a complete description of contrast for complex stimuli should include the anti-symmetric (quadrature) responses as well [2, 10]. This becomes obvious when C^L is computed for sinusoids, as shown in Figure 1. It can be seen that the contrast measured only with symmetric (in-phase) filters actually varies between $\pm C^M$ with the same frequency as the underlying sinusoid. This complicates establishing a correspondence between such a local contrast measure and data from psychophysical experiments on contrast sensitivity or masking, for example.

The in-phase and quadrature responses of an oriented filter, normalized by the low-pass response, for a natural test image are shown in Figure 2. Again it is evident that neither of the two is a good predictor of perceived contrast on its own, as both vary between negative and positive values of similar amplitude and exhibit zero-crossings right where the perceived contrast is actually highest.

These demonstrations underline the need for taking into account both the in-phase and the quadrature component in order to be able to relate a generalized definition of contrast to the Michelson contrast of a sinusoidal grating (i.e. a constant response across the whole image). Analytic filters represent an elegant way to achieve this. While their implementation in the one-dimensional case is straightforward, the design of general two-dimensional analytic filters is less obvious because of the difficulties involved in extending the Hilbert transform to two dimensions [9]. This problem is addressed in the next section on isotropic contrast.

Oriented measures of contrast can still be computed, though, because the Hilbert transform for filters whose angular support is smaller than π is well-defined. Such contrast measures are useful for many image processing tasks, because they can implement a multi-channel representation of low-level vision in accordance with the orientation selectivity of the human visual system and facilitate modeling aspects such as contrast sensitivity and pattern masking. They have been used in many vision models and their applications, e.g. in perceptual quality assessment of images and video [12]. Contrast pyramids have also been found to reduce the dynamic range in the transform domain, which may find interesting applications in image compression [11].

Lubin [3], for example, applies oriented filtering to C_j^L and sums the squares of the in-phase and quadrature responses for each channel to obtain a phase-independent oriented measure of contrast energy. Using analytic orientation-selective filters $\vartheta_k(x, y)$, this oriented contrast can be expressed as

$$C_{jk}^L(x, y) = \left| C_j^L * \vartheta_k(x, y) \right|. \tag{2}$$

Alternatively, an oriented pyramid decomposition can be computed first, and contrast can be defined by normalizing the oriented subbands with a low-pass band:

$$C_{jk}^O(x, y) = \frac{|\mathrm{bp}_j * \vartheta_k(x, y)|}{\mathrm{lp}_{j+2}(x, y)}. \tag{3}$$

As a matter of fact, both of these approaches yield quite similar results in a decomposition of natural images. However, some noticeable differences occur around edges of high contrast.

4. ISOTROPIC LOCAL CONTRAST

We now describe the construction of an *isotropic* contrast measure by combining analytic oriented filter responses. Isotropy can be important for applications where isotropic signals in an image are considered, e.g. spread-spectrum watermarking [13]. The main problem in defining an isotropic contrast measure based on filtering operations is that if we want a flat response to a sinusoidal grating as with Michelson's definition, we have to use 2-D analytic filters. This requirement makes it impossible to use a single isotropic filter. As already stressed in the previous section, the

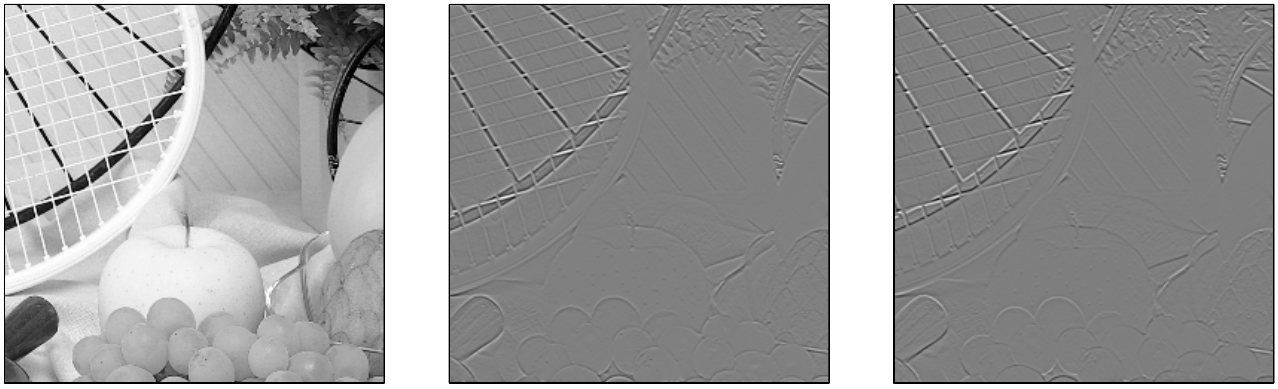

Figure 2: Test image (left) and normalized responses of oriented in-phase (center) and quadrature (right) filters.

main difficulty in designing 2-D analytic filters is that there is no real equivalent to the Hilbert transform in two dimensions. Instead, we have a series of transforms, the so-called *Riesz transforms* [9]; however, these are quite difficult to handle in practice. In order to circumvent this problem, we propose an approach using a class of non-separable filters that generalize the properties of analytic functions in 2-D. These filters are actually *directional* wavelets as defined in [1], which are square-integrable functions whose Fourier transform is strictly supported in a convex cone with the apex at the origin. It can be shown that these functions admit a holomorphic continuation in the domain $T = \mathbb{R}^2 + jV$, where V is the cone defining the support of the function. This is a genuine generalization of the Paley-Wiener theorem for analytic functions in one dimension. Furthermore, if we require that these filters have a flat response to sinusoidal stimuli, it suffices to impose that the opening of the cone V be less than π. This means that at least three of these filters are required to cover all possible orientations uniformly, but otherwise any number of filters is possible. Using a technique described in the appendix, we are able to design such filters in a very simple and straightforward way; we can even obtain dyadic oriented decompositions that can be implemented using a filterbank algorithm.

Working in polar coordinates (r, φ) in the Fourier domain, suppose we have a directional wavelet $\hat{\Psi}(r, \varphi)$ satisfying the above requirements and

$$\sum_{k=0}^{N-1} |\hat{\Psi}(r, \varphi - k\frac{2\pi}{N})|^2 = |\hat{\gamma}(r)|^2 \ , \qquad (4)$$

where $\hat{\gamma}(r)$ is the Fourier transform of an isotropic dyadic wavelet, i.e.

$$\sum_{j=-\infty}^{+\infty} |\hat{\gamma}(2^j r)|^2 = 1$$

and

$$\sum_{j=-J}^{+\infty} |\hat{\gamma}(2^j r)|^2 = |\hat{\phi}(2^J r)|^2 \ ,$$

where ϕ is the associated 2-D scaling function [4].

Now we can construct an isotropic contrast measure C_j^I as the square root of the energy sum of these oriented filter responses, normalized by a low-pass band:

$$C_j^I(x, y) = \frac{\sqrt{2\sum_k |\Psi_{jk} * f(x, y)|^2}}{\phi_j * f(x, y)} \ , \qquad (5)$$

where f is the input image, and Ψ_{jk} denotes the wavelet dilated by 2^{-j} and rotated by $2\pi k/N$. If the directional wavelet Ψ is in $L^1(\mathbb{R}^2) \cap L^2(\mathbb{R}^2)$, the convolution in the numerator of (5) is again a square-integrable function, and Eq. (4) shows that its L^2-norm is exactly what we would have obtained using the isotropic wavelet γ. As can be seen in Figure 4, C_j^I is thus an orientation- and phase-independent quantity, but being defined by means of analytic filters, it behaves as prescribed with respect to sinusoidal gratings (i.e. $C_j^I(x, y) \equiv C^M$ in this case).

An example of an oriented contrast pyramid decomposition is compared with the isotropic contrast pyramid in Figures 3 and 4. The oriented contrast pyramid using the contrast definition C_{jk}^O from Eq. (3) together with the corresponding wavelets is shown in Figure 3. As mentioned before, the contrast definition from Eq. (2) yields similar results overall with the exception of high-contrast edges. The corresponding isotropic contrast pyramid using the contrast definition C_j^I from Eq. (5) is shown in Figure 4. Comparing this contrast pyramid to the original image in Figure 2, it can be seen that the contrast features obtained with C_j^I correspond very well to the perceived contrast. The combination of the analytic oriented filter responses produces a meaningful phase-independent measure of isotropic contrast.

5. APPENDIX

We briefly explain the construction of an oriented dyadic wavelet pyramid starting from any continuous wavelet decomposition of $L^2\left(\mathbb{R}^2\right)$. First, suppose that ψ is an admissible isotropic 2-D wavelet, i.e. $\psi \in L^1\left(\mathbb{R}^2\right)$ and

$$0 < c_\psi = 2\pi \int_{\mathbb{R}^2} d^2\vec{\omega} \ \frac{|\hat{\psi}(\vec{\omega})|^2}{|\vec{\omega}|^2} < +\infty \, .$$

Then it is well known [6] that any signal $f \in L^2\left(\mathbb{R}^2\right)$ permits the following continuous wavelet expansion:

$$f = \int_{\mathbb{R}_*^+} \frac{da}{a^2} \int_{\mathbb{R}^2} d^2\vec{b}\ \langle \psi_{(\vec{b},a)}, f\rangle\ \psi_{(\vec{b},a)}\ , \tag{6}$$

where $\langle\,,\rangle$ is the L^2 scalar product, and

$$\psi_{(\vec{b},a)}(\vec{x}) = a^{-2}\psi\left(\frac{\vec{x}-\vec{b}}{a}\right).$$

The equality holds in L^2 sense. If the wavelet satisfies the (slightly) more restrictive condition

$$0 < \left| c_\psi = 2\pi \int_{\mathbb{R}^2} d^2\vec{\omega}\ \frac{\hat{\psi}(\vec{\omega})}{|\vec{\omega}|^2} \right| < +\infty\ ,$$

one has a simpler decomposition involving a scale integral only:

$$f = \int_{\mathbb{R}_*^+} \frac{da}{a^{3/2}}\, \langle \psi_{(\vec{b},a)}, f\rangle\, . \tag{7}$$

Even though Eqs. (6) and (7) involve continuous scaling and translations, they can be exactly discretized in order to fulfill the requirements of digital computing. In the linear case of Eq. (7) for example, one first introduces the scaling function

$$\hat{\phi}(\vec{\omega}) = \int_1^{+\infty} \frac{da}{a}\, \hat{\psi}(a\vec{\omega})$$

and the integrated wavelets

$$\begin{aligned} \hat{\Psi}(\vec{\omega}) &= \int_{1/2}^{1} \frac{da}{a}\, \hat{\psi}(a\vec{\omega}) \\ &= \hat{\phi}(2\vec{\omega}) - \hat{\phi}(\vec{\omega})\ . \end{aligned}$$

It is then easily verified that the following dyadic decomposition holds in L^2 sense:

$$f = \langle \phi_{(\vec{b},2^J)}, f\rangle + \sum_{j=-\infty}^{J} \langle \Psi_{(\vec{b},2^j)}, f\rangle\, . \tag{8}$$

Such a simple scheme allows us to build a very wide class of dyadic wavelet decompositions, and it has been shown [4,6] that these can be implemented in a very fast and efficient way using a pyramidal algorithm.

Finally, orientation selectivity is achieved by further decomposing $\hat{\Psi}$ using a partition of the circle. For this purpose, we introduce an infinitely differentiable compactly supported function η such that

$$\sum_{k=0}^{N-1} \eta\big(\varphi - k\frac{2\pi}{N}\big) = 1 \quad \forall \varphi \in [0, 2\pi]\, .$$

Using polar coordinates (r, φ) for the frequency vector $\vec{\omega}$, we then build N directional wavelets from the isotropic Ψ:

$$\hat{\Psi}_k\big(\vec{\omega}\big) = \hat{\Psi}\big(r\big)\eta\big(\varphi - k\frac{2\pi}{N}\big)\, .$$

This construction allows us to build oriented pyramids using a very wide class of wavelets. The properties of the filters involved in this decomposition can then be tailored for specific applications. In our case, spatio-frequency localization in dyadic oriented bands is achieved using wavelets Ψ_k that are a close approximation to Gabor filters, yet satisfying Eq. (8).

6. REFERENCES

[1] J.-P. Antoine et al.: "Directional wavelets revisited: Cauchy wavelets and symmetry detection in patterns." *Appl. Comp. Harm. Anal.* **6**(3), 314–345, 1999.

[2] J. G. Daugman: "Uncertainty relation for resolution in space, spatial frequency, and orientation optimized by two-dimensional visual cortical filters." *J. Opt. Soc. Am. A* **2**(7), 1160–1169, 1985.

[3] J. Lubin: "A visual discrimination model for imaging system design and evaluation." in *Vision Models for Target Detection and Recognition*, ed. E. Peli, pp. 245–283, World Scientific Publishing, 1995.

[4] S. Mallat, S. Zhong: "Characterization of signals from multiscale edges." *IEEE Trans. PAMI* **14**(7), 710–732, 1992.

[5] A. A. Michelson: *Studies in Optics*. University of Chicago Press, 1927.

[6] M. A. Muschietti, B. Torrésani: "Pyramidal algorithms for Littlewood-Paley decompositions." *SIAM J. Math. Anal.* **26**, 925–943, 1995.

[7] E. Peli: "Contrast in complex images." *J. Opt. Soc. Am. A* **7**(10), 2032–2040, 1990.

[8] E. Peli: "In search of a contrast metric: Matching the perceived contrast of Gabor patches at different phases and bandwidths." *Vision Res.* **37**(23), 3217–3224, 1997.

[9] E. M. Stein, G. Weiss: *Introduction to Fourier Analysis on Euclidean Spaces*. Princeton University Press, 1971.

[10] C. F. Stromeyer III, S. Klein: "Evidence against narrow-band spatial frequency channels in human vision: The detectability of frequency modulated gratings." *Vision Res.* **15**, 899–910, 1975.

[11] P. Vandergheynst, Ö. N. Gerek: "Nonlinear pyramidal image decomposition based on local contrast parameters." in *Proc. Nonlinear Signal and Image Processing Workshop*, Antalya, Turkey, 1999.

[12] S. Winkler: "Issues in vision modeling for perceptual video quality assessment." *Signal Processing* **78**(2), 1999.

[13] S. Winkler, M. Kutter: "Vers un tatouage à étalement de spectre optimal utilisant le système visuel humain." in *Proc. CORESA Workshop*, pp. 25–33, Sophia Antipolis, France, 1999, invited paper.

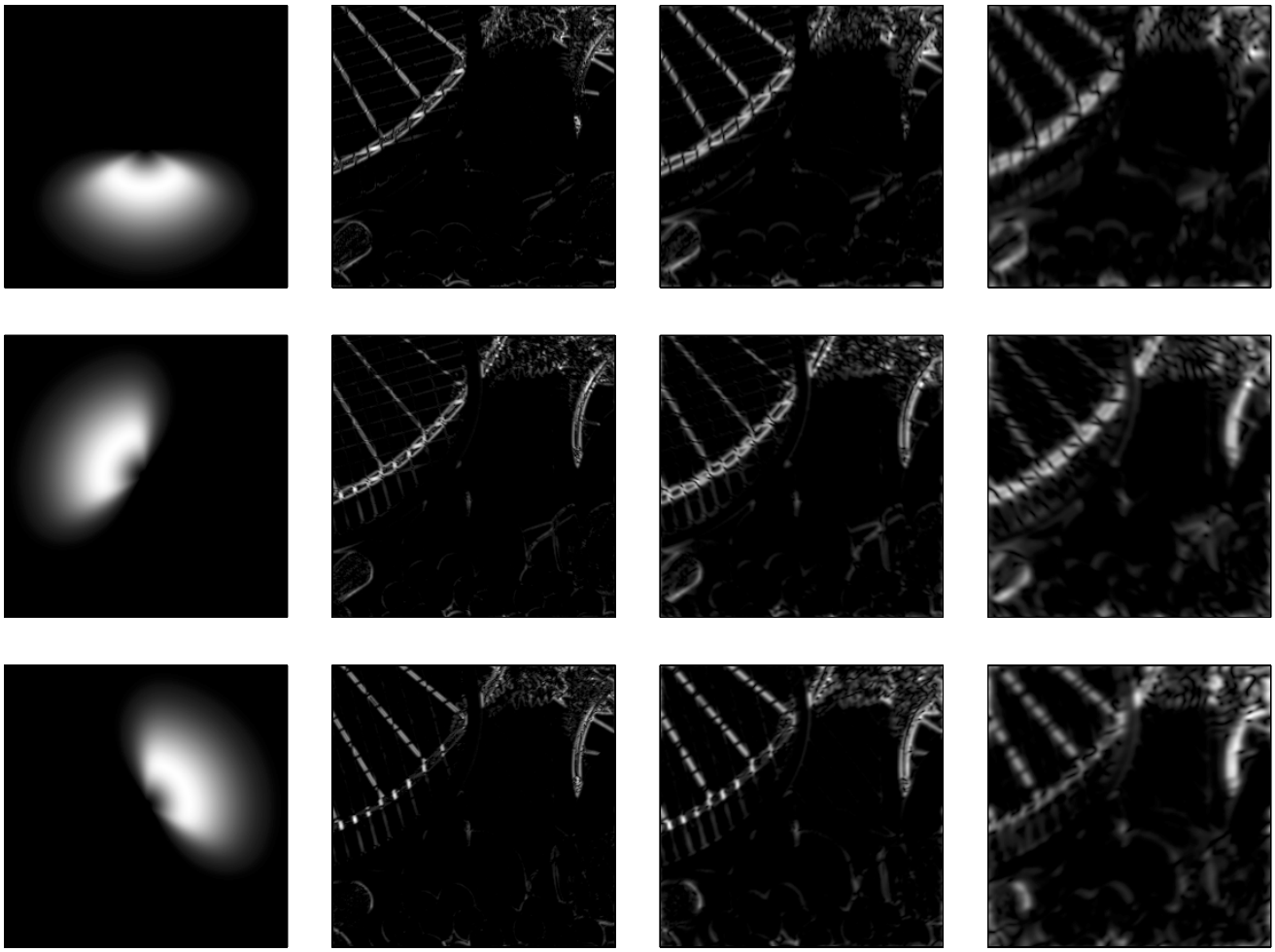

Figure 3: Oriented contrast of the test image from Figure 2. The left column shows the three analytic directional wavelets $\hat{\Psi}(r, \varphi - k\frac{2\pi}{N})$ of the decomposition, which are applied to obtain the oriented contrast $C^O_{jk}(x, y)$ at three different scales j shown in each row.

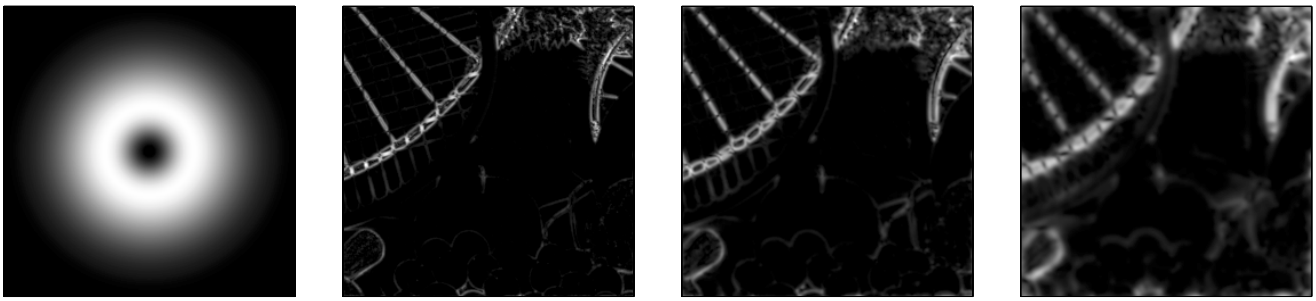

Figure 4: Isotropic contrast of the test image from Figure 2. The energy sum of the three directional wavelets from Figure 3 as given by Eq. (4) is shown on the left. The oriented filter responses are combined as described in Eq. (5) to yield the isotropic contrast $C^I_j(x, y)$, shown here at three different scales.